Electronic Supplementary Material (ESI) for ChemComm.
This journal is © The Royal Society of Chemistry 2022

Supporting Information

Hollow and nanoporous Ag sub-microcubes as SERS substrates

Lihua Feng, Yumeng Zhou, Wenqin Wang*

School of Materials Science and Chemical Engineering, Ningbo University, Ningbo 315211, P. R. China.

*Corresponding author: Wenqin Wang, E-mail address: wqwang@126.com

EXPERIMENTAL SECTION

Chemicals

Silver nitrate ($AgNO_3$, 99.8%), ammonium hydroxide solution ($NH_3•H_2O$, 25%), sodium borohydride ($NaBH_4$), trisodium citrate ($Na_3C_6H_5O_7$; Na_3Cit), poly(vinyl pyrrolidone) (PVP, M_w = 550 000), Rhodamine 6G (R6G) and thiram (97%) were obtained from Sinopharm Chemical Reagent Co. (Shanghai, China). NH_2-terminated silicon wafers were obtained according to our previous report.[1] All chemicals were used as received without further purification.

Fabrication of micrometer-sized $Ag(NH_3)_2NO_3$ cubes

First, the ammonia solution was slowly added to silver nitrate solution with appropriate concentrations to form a transparent silver ammonia complex solution according to the following reaction [2]:

$$AgNO_3 + 2NH_3•H_2O = Ag(NH_3)_2NO_3 + 2H_2O$$

Then, a few droplets of freshly prepared silver ammonia complex solution were dripped to a NH_2-terminated silicon wafer. Subsequently, the substrate was placed in an oven set at 20 °C and allowed to slowly evaporate the droplets for 45-60 min to form micrometer-sized cubic crystals.

Fabrication of Ag_3Cit sub-microcubes and hollow and nanoporous Ag sub-microcubes

The $Ag(NH_3)_2NO_3$ microcubes on silicon wafers were immersed in Na_3Cit aqueous solution for different times to form $Ag_3C_6H_5O_7$ (Ag_3Cit) nanocubes. Then, the substrates were taken out, washed with deionized water, and re-immersed in PVP aqueous solution (0.02 g/mL) for 3 h, ensuring that the surface of each Ag_3Cit sub-microcube was effectively covered by PVP. Finally, the substrates were immersed in $NaBH_4$ aqueous solution (0.01M) for different times. After the reaction, the products were rinsed with deionized water and dried.

SERS performances of hollow and nanoporous Ag sub-microcubes

20 μL of R6G solution with different concentrations was dropped onto hollow and nanoporous Ag

sub-microcubes. Subsequently, the SERS substrates were rinsed with ethanol and dried by N_2 flow for SERS measurements.

In order to investigate the practicality of the Ag sub-microcubes on detecting thiram residues, the following tests were carried out. A total of 20 μL of thiram solution with various concentrations (1000 ng/mL to 10 μg/mL) were dripped on the Ag sub-microcubes surface, then dried by N_2 flow.

The SERS spectra were obtained by focusing a 1 μm laser spot on the samples by using a 20× objective lens, and accumulated three times for 10 s each.

Characterization

SEM images of the products were obtained by a FEI Nova NanoSEM 450 scanning electron microscopy, operating at 5 kV. High-resolution transmission electron microscopy (HRTEM) and selected area electron diffraction (SAED) were conducted by a FEI Tecnai F20 transmission electron microscope, operating at 100 kV. The X-ray diffraction (XRD) patterns were obtained with a Bruker D8 ADVANCE with Cu Kα irradiation source (λ=1.5418 Å). Raman signals were recorded with a confocal microscopy Raman spectrometer (Renishaw inVia-reflex) with 633 nm laser source.

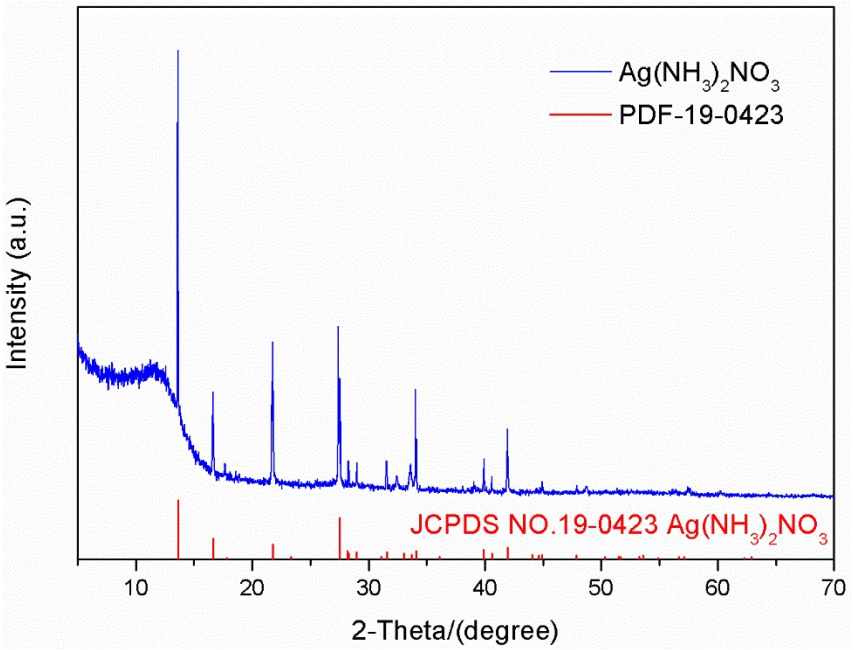

Fig. S1 XRD pattern of $Ag(NH_3)_2NO_3$ microcubes and the standard pattern of $Ag(NH_3)_2NO_3$.

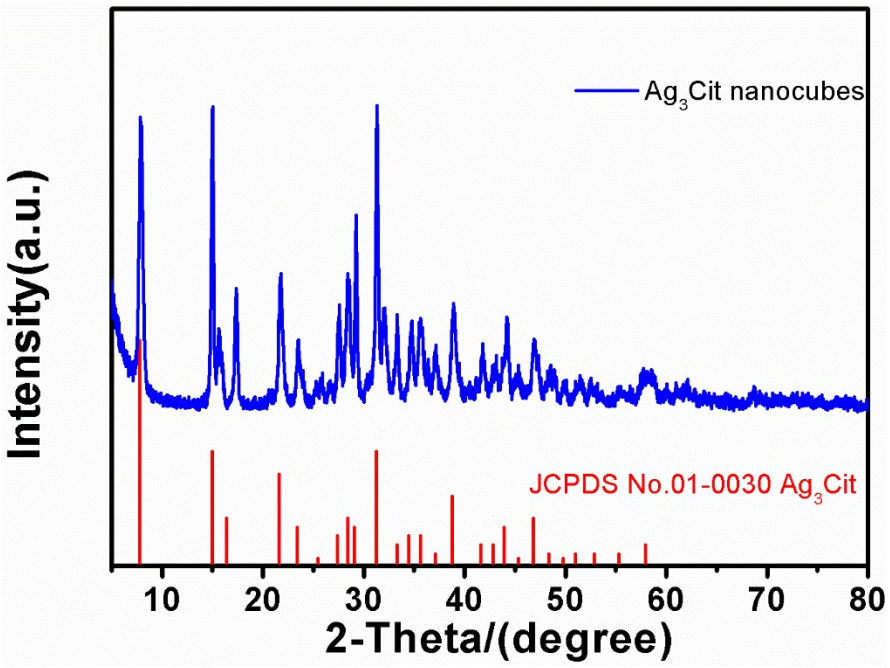

Fig. S2 XRD pattern of the as-prepared products and the standard pattern of Ag_3Cit.

The actual formation mechanism of Ag_3Cit sub-microcubes is not yet clear, a hypothesis is proposed and the schematic illustration of formation process of the Ag_3Cit sub-microcubes is shown in Fig.S3.

When the $Ag(NH_3)_2NO_3$ microcubes were immersed in Ag_3Cit aqueous solution, first, the surface of the $Ag(NH_3)_2NO_3$ crystals began to dissolve in aqueous solution and $[Ag(NH_3)_2]^+$ ions were released. Then Cit^{3-} ions reacted with $[Ag(NH_3)_2]^+$ ions to form Ag_3Cit crystals on the surface of the dissolving $Ag(NH_3)_2NO_3$ crystals. Because of the surface dissolution, the smooth surface of the original $Ag(NH_3)_2NO_3$ crystal became spiky and fissures were observed. As the dissolution lasted, more $Ag(NH_3)_2]^+$ ions were released and more Ag_3Cit crystals were obtained. In this process, the $Ag(NH_3)_2NO_3$ crystals slowly dissolved, which controlled the release rate of the $Ag(NH_3)_2]^+$ ions and growth rate of Ag_3Cit crystals. This controlled growth rate of Ag_3Cit crystals may cause the resultant products with uniform cubic structures.

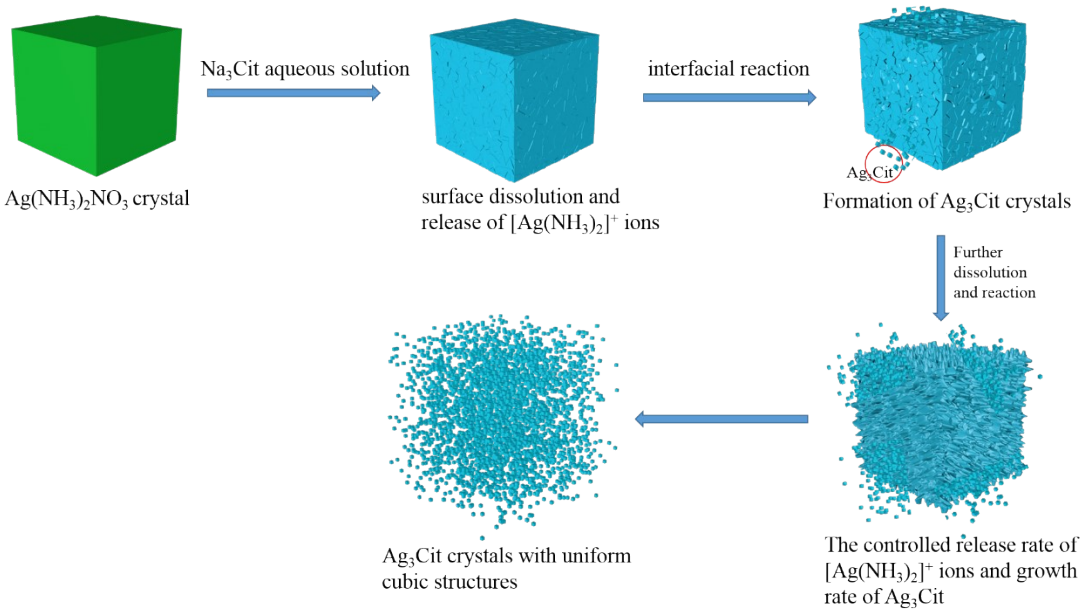

Fig. S3 Schematic illustration of the formation process of the Ag_3Cit sub-microcubes.

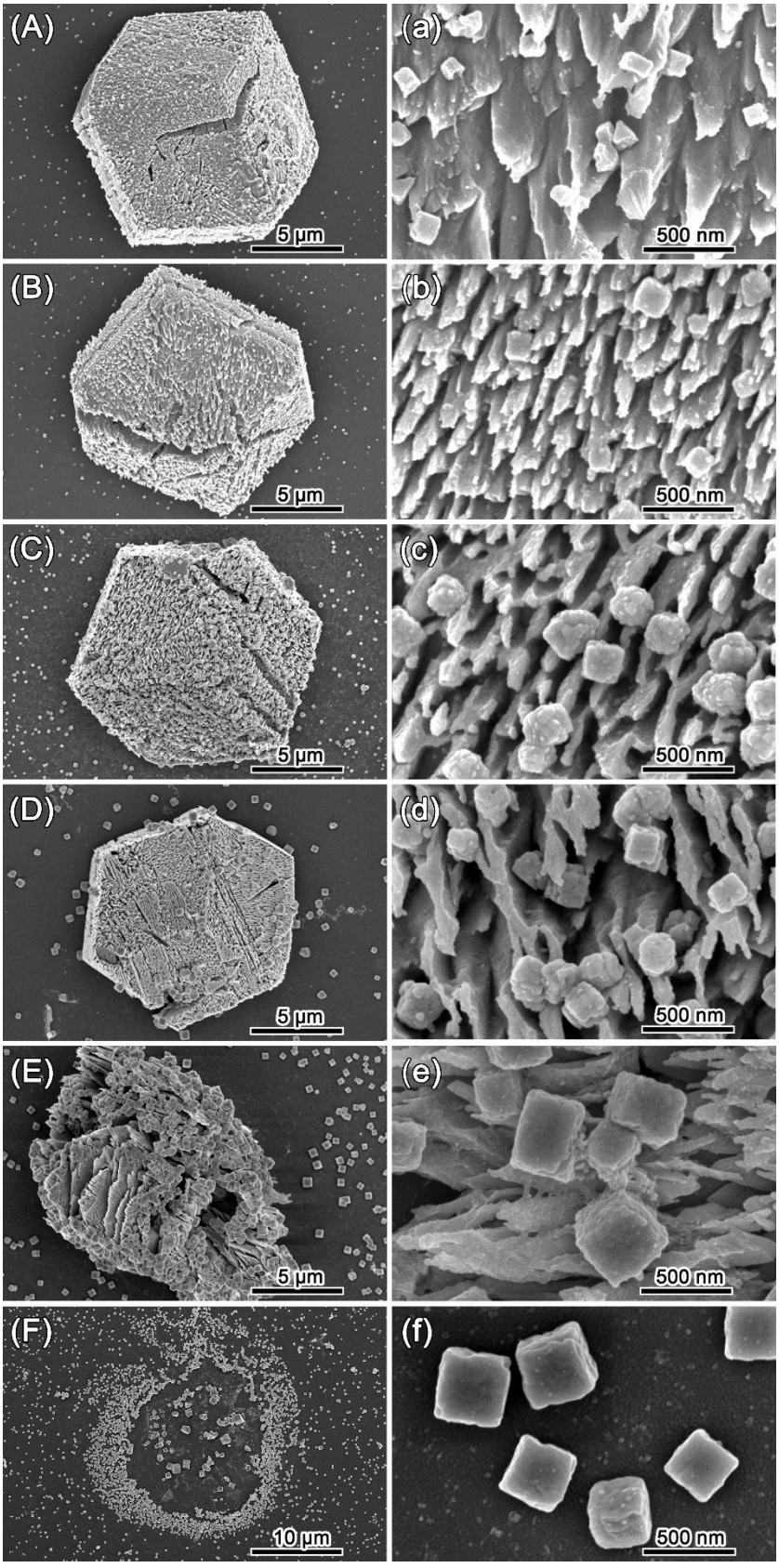

Fig. S4 SEM images of a $Ag(NH_3)_2NO_3$ microcube in Na_3Cit solution (0.05 M) for 90 s (A,a)，10 min (B,b)，30 min (C,c)，1 h (D,d)，3 h (E,e), and 6 h (F,f).

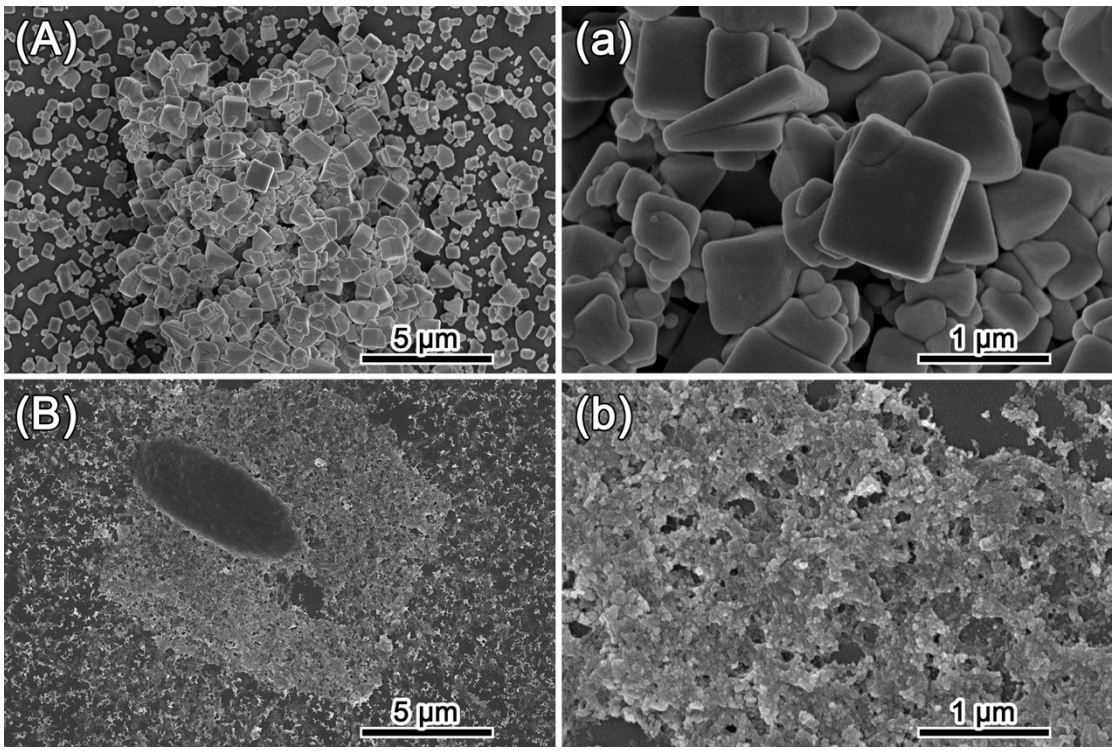

Fig. S5 Low- and high magnification SEM images of a $Ag(NH_3)_2NO_3$ microcube in Na_3Cit solution (0.01 M) for 6 h at different reaction temperature: 30 ^oC (A,a) and 50 ^oC (B,b), respectively.

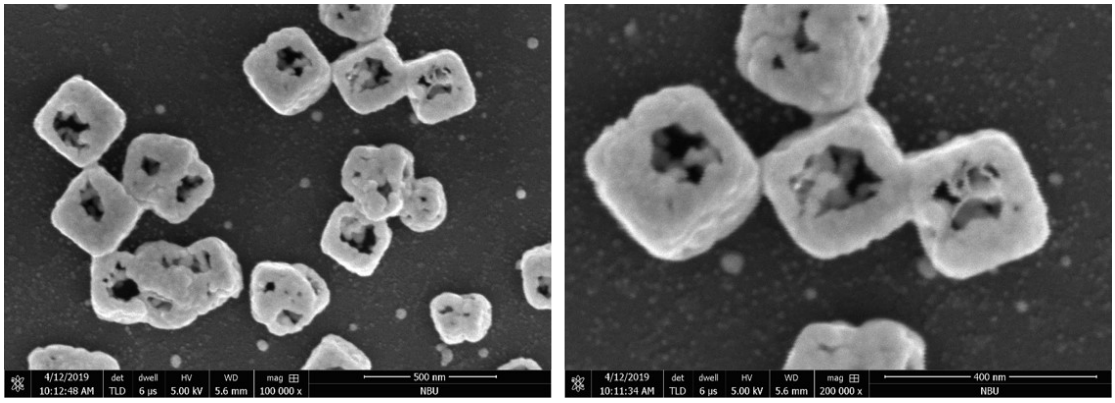

Fig. S6 SEM images of Ag_3Cit cubes in $NaBH_4$ solution (0.01M) for 2 h.

The four SAED rings can be approximately indexed to the {111}, {200}, {220}, and {311} lattice planes of silver (Fig. S7B). The high-resolution TEM (HRTEM) micrograph shows two randomly oriented nanocrystals in the selected part, which are agreement with the SAED results. Two kinds of lattice spaces are measured to be 0.0236 and 0.0204 nm, which can be indexed to (111) and (200) planes of silver, respectively (Fig. S7C).

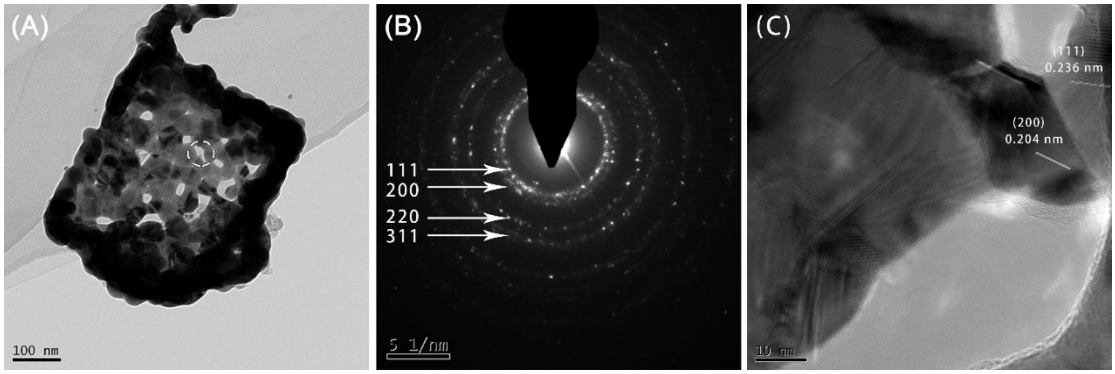

Fig. S7 TEM image of an individual Ag cage (A). SAED pattern (B), and HRTEM image obtained from the circled region (C).

The XRD pattern of the silver sub-microcages is shown in Fig.S8. Five peaks at 38.1°, 44.3°, 64.4°, 77.4°, and 81.5°, which are respectively assigned to the (111), (200), (220), (311), and (222) phases of the face-centered cubic crystal structure of Ag NPs (JCPDS File Card No. 04-0783).[3]

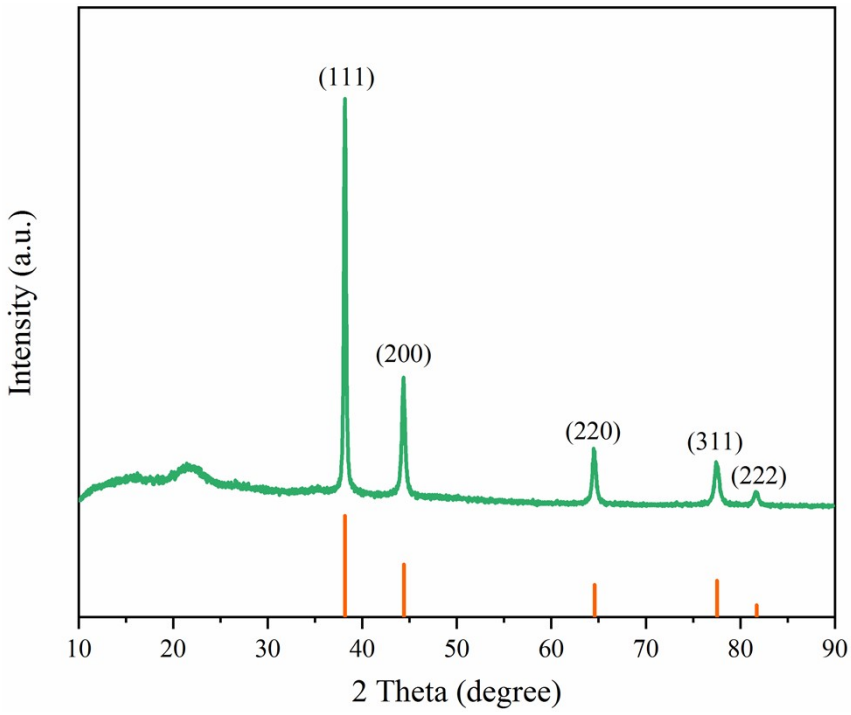

Fig. S8 XRD pattern of the Ag sub-microcages.

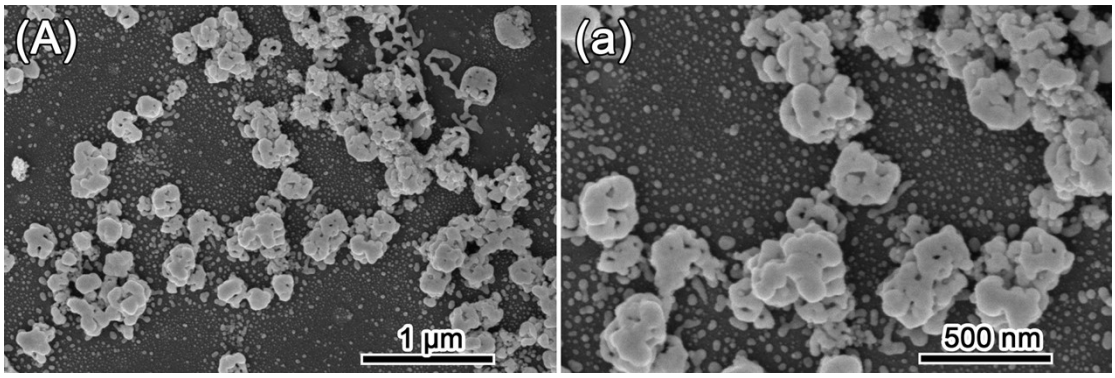

Fig. S9 Low- and high magnification SEM images of the obtained products (Ag_3Cit sub-microcubes without modifying with PVP in $NaBH_4$ aqueous solution for 1 h at room temperature).

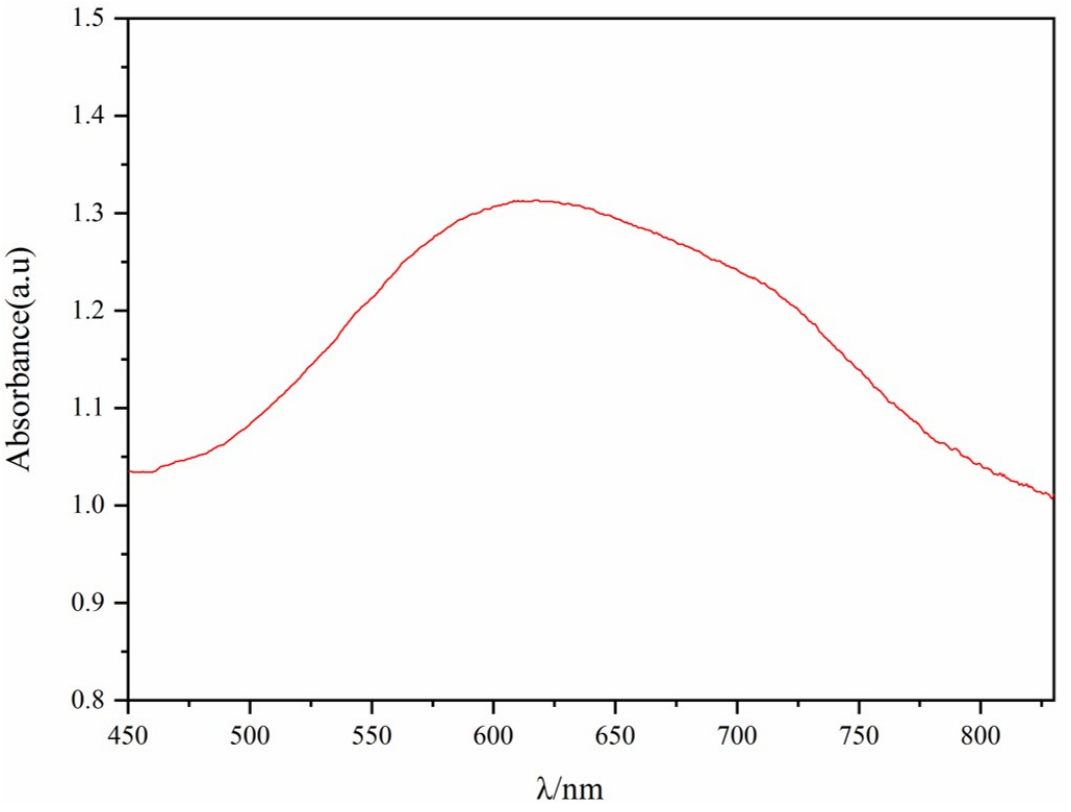

Fig. S10 UV-vis spectrum of Ag sub-microcages on the Si substrate.

Quantitative comparison of the SERS intensities as a function of R6G concentration demonstrates that a linear SERS response can be obtained over R6G concentrations ranging from 10^{-10} to 10^{-6} M. Below 10^{-11} M, R6G molecules are randomly deposited on the Ag particles, forming submonolayer aggregates on the substrate. With decreasing concentrations, the occurrence of such aggregates decrease correspondingly. Consequently, SERS signals are collected from these isolated submonolayer aggregates over the concentration range of 10^{-11} to 10^{-16} M, leading to similar signal intensities observed despite large concentration changes.[4]

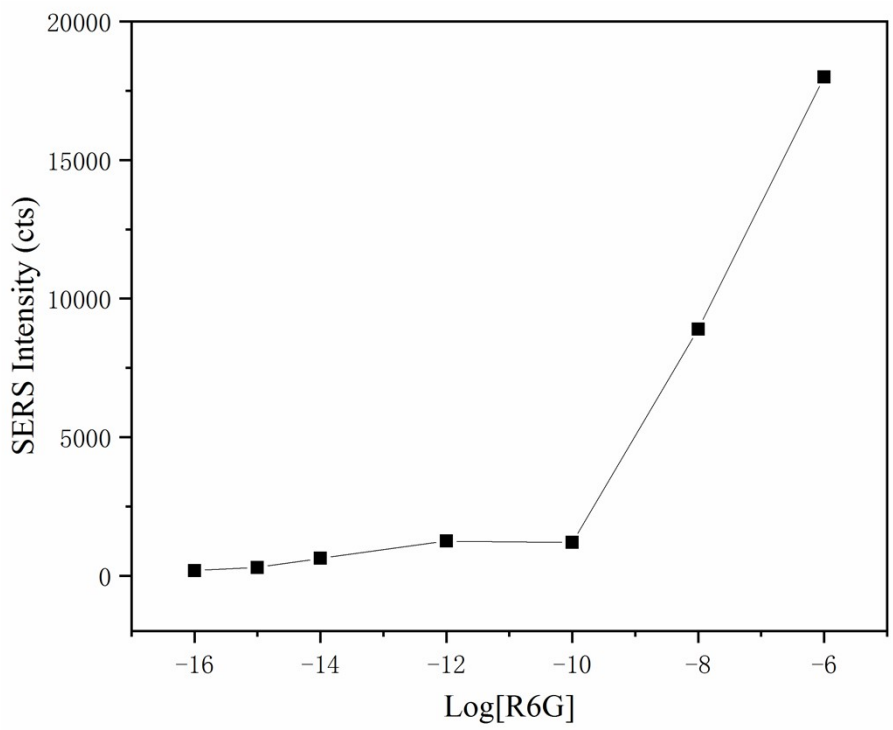

Fig. S11. SERS intensities at 610 cm^{-1} for R6G concentration ranging from 10^{-6} to 10^{-16} M.

We determined the SERS intensities of six trials to illustrate the reproducibility of Ag sub-microcages for detection of R6G concentration (10^{-16} M). From Fig.S12, all of the six SERS intensities at 610 cm^{-1} exceed 100 counts, one of the criteria to be considered as a distinguishable signal.

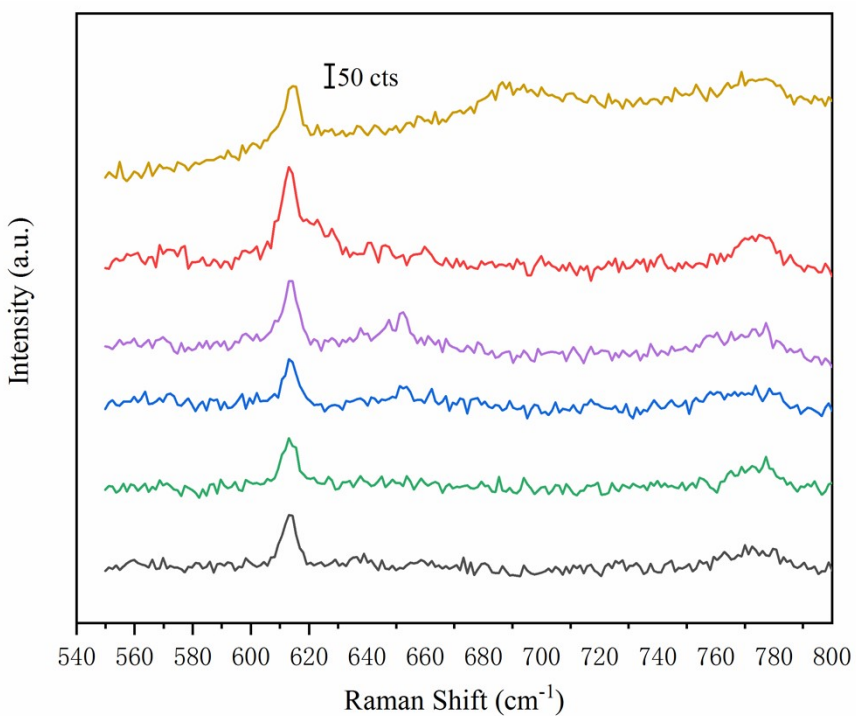

Fig. S12 SERS spectra of R6G solution with ultra-low concentration (10^{-16} M) on Ag sub-microcages for six trials.

Fig. S13A shows the Raman spectrum of 10^{-4} M R6G. The Raman intensities at 610 cm^{-1} for R6G solution (10^{-16} M) on Ag sub-microcages were obtained from Fig.S12 and exhibited in Figure S13B. Based on Fig. S12B, an average Raman intensity at 610 cm^{-1} (about142 cts) was obtained.

Detail calculation of SERS enhancement factor is shown below:

$$EF = [(I_{SERS}) / (I_{Raman})] \times [(C_{Raman}) / (C_{SERS})]$$

$$= (142 / 335) \times (10^{-4} / 10^{-16})$$

$$= 4.2 \times 10^{11}$$

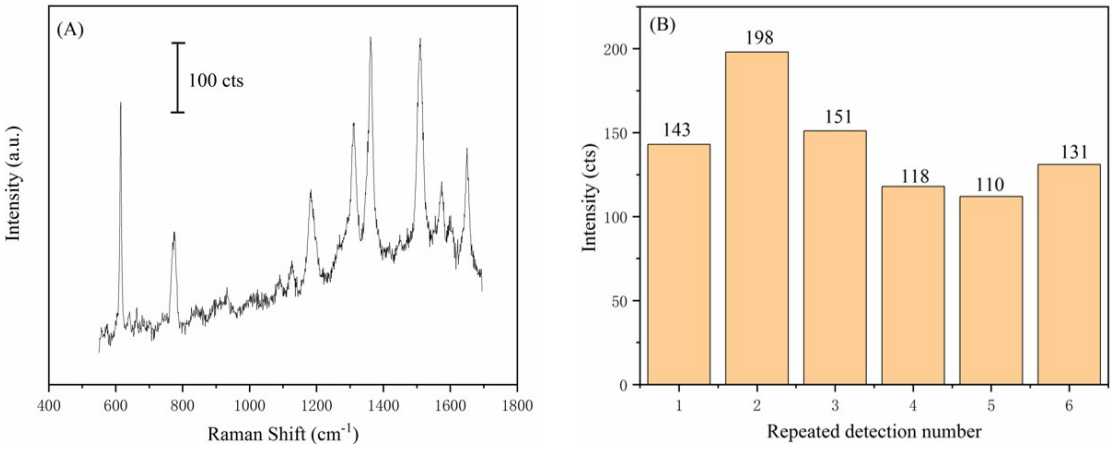

Fig. S13 (A) Raman spectrum of R6G solution with concentration of 10^{-4} M on Si substrate. (B) SERS intensities at 610 cm^{-1} for R6G solution (10^{-16} M) on Ag sub-microcages.

Thiram, a dithiocarbamate (DTC) pesticide, is widely used during the growth of fruits and vegetables. However, its extensive use and residues can pose a risk to human beings.[5]

Fig. S14A shows SERS signals of thiram with different concentrations on Ag sub-microcages. The corresponding SERS spectra exhibit distinct representative peaks at 933, 1144, 1381, and 1510 cm^{-1}, representing the characteristic vibrations of thiram.[6] The limit of detection (LOD) is assessed to be 10 ng/mL. The calibration curve illustrated in Fig. S14B displays a good linear relationship between the Raman intensity at the peak of 1381 cm^{-1} with linearly dependent coefficient ($R^2 = 0.991$).

Stability is a significant parameter for SERS-active substrates in practical application. Time-dependent SERS measurements were conducted. Fig. S14C shows SERS spectra of thiram, obtained from Ag sub-microcages when exposed under ambient conditions with durations of 0, 7, 15, 30 and 45 days, wherein the signal intensities of the sample would decay with different degrees after different exposure periods. During the initial exposure time of 7 days, the signal intensity of Ag sub-microcages at 1381 cm^{-1} decreased by about 61%. After 45 days, the SERS intensity of Ag sub-microcages decreased with 25%, due to the unavoidable oxidation of Ag.[7]

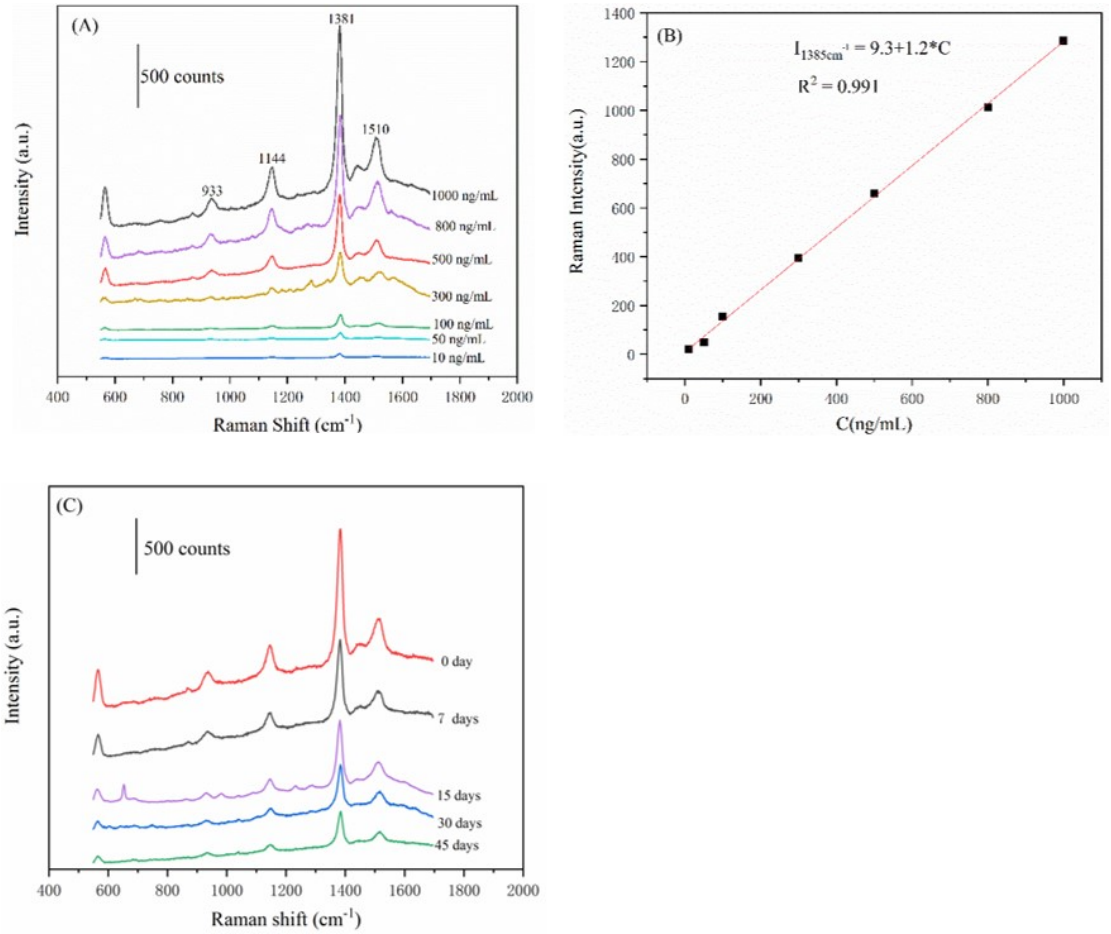

Fig. S14 (A) SERS spectra of thiram solution with different concentration from 10 to 1000 ng/mL detected on Ag sub-microcages. (B) Linear correlation of Raman intensity at 1381 cm^{-1} with the concentration of thiram. (C) SERS spectra of thiram solution (1000 ng/mL) on Ag sub-microcages exposed to ambient condition with different periods.

REFERENCES

(1) Y. Q. Yang, W. Q. Wang, T. Chen and Z.-R. Chen, *ACS Appl. Mater. Interfaces,* 2014, **6**, 21468-21473.

(2) Y. P. Bi, H. Y. Hu, S. X. Ouyang, G. X. Lu, J. Y. Cao and J. H. Ye, *Chem. Commun.,* 2012, **48**, 3748-3750.

(3) S. P. Dubey, A. D. Dwivedi, I.-C. Kim, M. Sillanpaa, Y.-N. Kwon and C. Lee, *Chem. Eng. J.* 2014, 244, 160-167.

(4) H. K. Lee, Y. H. Lee, Q. Zhang, I. Y. Phang, J. M. R. Tan, Y. Cui and X. Y. Ling, *ACS Appl. Mater. Interfaces,* 2013, 5, 11409-11418.

(5) K. Wang, X. Zhang, C. Niu and Y. Wang, *ACS Appl. Mater. Interfaces,* 2014, **6** 1272-1278.

(6) J. Zhu, Q. Chen, F. Y. H. Kutsanedzie, M. Yang, Q. Ouyang and H. Jiang, *Anal. Methods*, 2017, **9**, 6186−6193.

(7) C.-Y. Zhang, R. Hao, B. Zhao, Y. Fu, H. Zhang, S. Moeendarbari, C. S. Pickering, Y.-W. Hao and Y-Q. Liu, *Appl. Surf. Sci.,* 2017, **400**, 49-56.